SciEn
Journal of Engineering Advancements Vol. 03(04) 2022, pp 144-154 https://doi.org/10.38032/jea.2022.04.002

Investigation on Circular Array of Turbulent Impinging Round Jets at Confined Case: A CFD Study

Sudipta Debnath[1,], Md. Tanvir Khan[2], Zahir Uddin Ahmed[1]*

[1]Department of Mechanical Engineering, Khulna University of Engineering & Technology, Khulna – 9203, Bangladesh.
[2]Department of Mechanical and System Engineering, Okayama University, Okayama – 700-8530, Japan

Received: September 27, 2022, Revised: December 12, 2022, Accepted: December 14, 2022, Available Online: December 23, 2022

ABSTRACT

Jet impingement has immense applications in industrial cooling, such as glass tempering, turbine blades, electrical equipment, etc. The interplay in-between several jet arrangements and the effect of swirl intensity require enormous study to achieve steady heat transfer. This paper numerically investigates an inline array of 25 circular confined swirling air jets impinging vertically on a flat surface. In this regard, three-dimensional simulations are executed using the finite volume method for a number of control parameters, such as Reynolds number (Re = 11600, 24600, and 35000), impinging distance (H/D = 0.25, 0.5, 1), swirl number (S = 0.3 and 0.75) and jet-to-jet separation distance (Z/D = 2.5), where, D is the nozzle diameter. Impinging pressure distribution, flow velocity, surface Nusselt number, and Reynolds stresses are investigated for different operating conditions. The results reveal that both the wall pressure and surface Nusselt number are comparatively uniform in the case of high swirl flow. Moreover, distinct heat transfer behavior is observed from the unconfined condition for high swirl flow in which the heat transfer is constant after a certain radial distance. The Reynolds normal stress adjacent to the nozzle exit is more rigorous than the downstream regions while Reynolds shear stress varies unpredictably along the radial direction. In addition, an estimated 102 % enhancement in average Nusselt number is observed for high swirl flow, at a Reynolds number increment from 11600 to 35000. This enhancement is evident by 23 % in terms of thermal performance factor. Besides, the average Nusselt number and thermal performance factor augmented by 19 % and 8 %, respectively, for an increased swirl intensity at low a Reynolds number (Re = 11600).

Keywords: Thermal Performance Factor, Pressure Coefficient, Swirl, Reynolds Stress, CFD.

1 Introduction

Jet impingement is a common method of heating or cooling solid surfaces. The heat transfer rate by the impinging jet is usually higher than the other conventional methods. Because the flow of fluid in the form of a jet impingement rapidly increases its momentum. In turbulent flow, the molecules in the flowing fluid act in a random manner. Molecules in a flowing fluid transfer momentum and energy from one place to another by mixing fluid particles often called vortex mixing. Usually, the heat transfer rate in turbulent flow is high due to rising and random mixing. Therefore, the most practical use of jet impact is in industries where heat transfer requirements are greater than the capacity of conventional heating and cooling techniques. Industrial jet impingement includes drying of paper, textiles, and veneer, tempering of glass, annealing of metals and cooling of gas turbine blades, electronic components and drying of films in the film industry, application of steam to the cylindrical surfaces of the combustion chamber [1]-[5].

Martin [6] measured average mass transfer under multiple confined slot jets. In his study, the outflow was reserved to exit only in the traverse direction through the open sides at the ends of the slot nozzles and the transport rate at the impingement plate was highly nonuniform in the direction of the nozzle length. Colucci, et al. [7] implemented a thermochromatic liquid-crystal technique and examined the effects of hyperbolic nozzle geometry on the local heat-transfer coefficients for confined impinging air jets. They reckoned that the local heat-transfer coefficients for confined jets are more sensitive to Reynolds number and nozzle-to-plate spacing than those for unconfined jets. Saad, et al. [8] investigated multiple confined impinging slot jets without crossflow effects and observed that the heat-transfer data acquired for unconfined jets cannot be employed reliably in the design of confined jets. Huber, et al. [9] studied convective heat transfer to a confined impinging array of air jets with spent air exits with the implementation of bandpass filters and an electronic digitizer board. Their results have shown that the inclusion of spent air exits increased the convective heat transfer coefficient and changed the location of the optimal separation length.

Markal [10] experimentally investigated heat transfer characteristics and wall pressure distribution of swirling coaxial confined turbulent impinging air jets at multiple nozzle-to-plate distances and flow rates for a constant total flow rate. He observed that the flowrate ratio improves the uniformity of heat transfer through the impingement surface and works better for lower impinging distance. Also in terms of pressure distribution, there are subatmospheric regions near the impact plate. He further investigated the effect of multiple total flow rates on the thermal management ability of swirling coaxial confined impinging air jets and found that both heat transfer rate and radial uniformity are improved by increasing total flow rate [11]. Habib, et al. [12] studied velocity characteristics of both non-swirl and swirl confined coaxial jets. Their results show, with swirl, the area near the recirculation of the center line and between one and three diameters of the furnace below the exit plane. Thus, as the number of swirls increases from zero, this chance of recirculation increases and is finally met. Memar, et al. [13] studied convective heat transfer data from a confining tube to coaxial, counter-swirled jets and observed that peak Nusselt

*Corresponding Author Email Address: sudiptadebnath913@gmail.com

number was shifted upstream with the increase of inner jet swirl strength. Petera, et al. [14] studied both experimentally and numerically heat transfer measurements of a confined impinging jet with a tangential velocity component. They found that the addition of the tangential velocity component significantly influences the velocity field and the intensity of heat transfer in the stagnant region compared to the classical characteristics of the impinging jet. Shuja, et al. [15] investigated confined swirling jet impingement onto an adiabatic wall and found that with the increase of swirl velocity, the jet axis tilts towards the radial direction.

In order to improve convection heat transfer and minimize defects, a plethora of research has been performed to determine the effect of different parameters on multiple jet impingement flow dynamics and heat transfer. Chouaieb et al. [16] investigated the effect of a swirl generator on the mixing process using numerical simulation and found that the position of the swirl generator had a clear effect on the mixing process. Liu et al. [17] predicted the swirl length of different vortex patterns by studying the swirling flow of gas and fluid caused by fan-type vortexing in a vertical duct. The swirl length of the swirling gas column and the swirling intermittent flow increases as the surface velocity of the liquid increases or as the surface velocity of the gas decreases. Yan et al. [18] described a numerical method for investigating the uniform structure and components of turbulence associated with vortex-vortex interactions. He found that under medium and high swirl intensities, the turbulence intensity was enhanced and weakened, respectively, from the single swirling jet level, and augmented and depressed, respectively, by enlarging the jet-to-jet spacing. Fenot et al. [19] studied the flow field of the swirling impinging jets with eight channels for Re = 23,000–33,000. He believed that the internal shear layer caused the mainstream to accelerate, and vortices formed under the mainstream increased Nusselt number by 50%. Ahmed et al. [20], [21] studied the influence of inflow profile and swirl intensity on the development of turbulent impinging jets. Compared to the non-swirling jet, the turbulence kinetic energy and shear stress of the wall are significantly reduced when the weak swirling flow enters the impinging jet. Wu et al. [22] found that the pressure distribution in the four composite cooling structures was very different from swirl cooling and impingement cooling. In addition, the nozzle-nozzle mass flow ratio distribution changes with changing nozzle position, which affects flow and heat transfer characteristics. Debnath et al. [23]-[25] investigated the average flow and pressure characteristics of both swirling and non-swirling jet arrays. The results show that the swirling jet backflow intensity is greater than the non-swirling jet and provides the maximum pressure coefficient at the stagnation point of each jet. Wannassi et al. [26] studied the details of flow and the complex flow structure of a staggered combination of straight and swirling jets. They believe that the vortex rapidly disappears in the circumferential direction below the nozzle outlet, which results in an insufficient axial impulse.

Hollworth et al. [27] investigated the heat transfer field of jet impact cooling with emission holes on the target surface. They compared their results in cases without outlets and found that the nozzle field with outlets had a 20-30% higher heat transfer rate. Zhang et al. [28] compared the cooling performance of hybrid impingement cooling and effusion cooling of a multi-swirler combustor and concluded that the hybrid impingement cooling method was very effective. Wu et al. [29] investigated an array jet impingement cooling for a simulated chip using an additively manufactured manifold design that encloses the chip with working fluid. They created a series of extraction holes between adjacent nozzle holes to prevent cross-flow and nozzle interference between adjacent nozzles in their design. In short, extracting spent flow improves the heat transfer performance of the jet cooling field. Caliskan and Baskaya [30] investigated heat transfer in an inline jet array on smooth and rib-roughened surfaces. Through their analysis, they found an increase in the heat transfer coefficient over the surface from 4% to 26% when compared with a flat plate. Chauhan and Thakur [31] studied the heat transfer and friction factor correlations for impinging jets and observed that, the streamwise and spanwise jet-to-jet spacing enhanced the heat transfer rates.

Hatami et al. [32] performed a two-dimensional (2D) computational fluid dynamics (CFD) simulation of air-jet using two different turbulence models and found that heat transfer could be improved by almost 30% in an unconfined test case compared to a confined one. A large impact of dimensionless length was also observed in achieving maximum heat transfer. C. Wang et al. [33] experimentally investigated the air jet with uniform constant heat flux boundary condition and found that air velocity near the impact area was an important factor in improving heat transfer. Katti et al. [34] conducted experimental measurements of single free jet heat transfer and Jeffers et al. [35] examined the stagnation zone with a single confined and submerged impinging jet. Both of them noticed that stagnant pressure could migrate to the exit of the nozzle and change the nozzle outlet velocity profile in the proximity of the nozzle exit. Ekkad and Han [36] demonstrated transient liquid crystal thermography techniques and other gas turbine cooling technologies. Their work reveals important details of the two-dimensional heat transfer distribution. Ichikawa et al. [37] investigated the flow behavior of a series of circular jets by varying the nozzle to plate distance and nozzle to nozzle distance and found that heat transfer performance was increased by a configuration that included nozzle to plate distance 2 and nozzle to nozzle distance 4. Buzzard et al. [38] and Ligrani et al. [39] studied the impact of a rough surface in the jet impingement field and found an increase in surface heat transfer and surface Nusselt number for both laminar and turbulent flow.

Although unconfined impinging jets are widely available in the literature, possibly due to their huge applicability to industrial applications and uncomplicated correlation with experimentations, in numerous functional applications heat transfer operations are applied in a confined atmosphere. Nevertheless, a few number of research has been conducted on confined impinging jets, which are often limited to non-swirl flow [35], [40]–[42]. The results show significantly different behavior of flow and heat transfer compared to their unconfined complements. Research on swirling impinging jets with flow confinements is poor in the literature. Thus, this paper will investigate the basic thermo-fluidic behavior of multiple swirling impinging jets due to the flow confinement at very small impingement distances (H/D = 0.25, 0.5, 1) for three different Reynolds numbers equal to 11,600, 24600, and 35000, at a jet-to-jet spacing Z/D = 2.5. The degree of swirl intensity is varied from medium to the highest (S = 0.3 and 0.75).

2 Methodology

A multiple swirling air jet impingement system consisting of twenty-five circular jets and a flat round surface is considered in this study. The jets emanate from an axial-plus-tangential aerodynamic swirl nozzle of diameter 40 mm in which a seamless transition from no swirl to high swirl flow can be

achieved for the identical mass flow rate. The detailed dimension of this nozzle is available in Islam et al. [43] and Khan et al. [44], [45], hence is not repeated here for brevity. The nozzles are organized in an inline arrangement and evenly distributed into three concentric circles around a central nozzle with 8 nozzles in each circle. Due to the symmetrical nature of the problem, only a quarter of the full domain was considered for the simulation to save computational costs. The physical arrangement of the nozzle array along with the coordinate setup of the computational domain and a representative schematic diagram of the swirling jet flow structure is illustrated in Fig. 1. Such a physical system is applicable to the glass tempering process in which multiple jets are used for the rapid cooling of the tempered glass after numerous heat treatment operations.

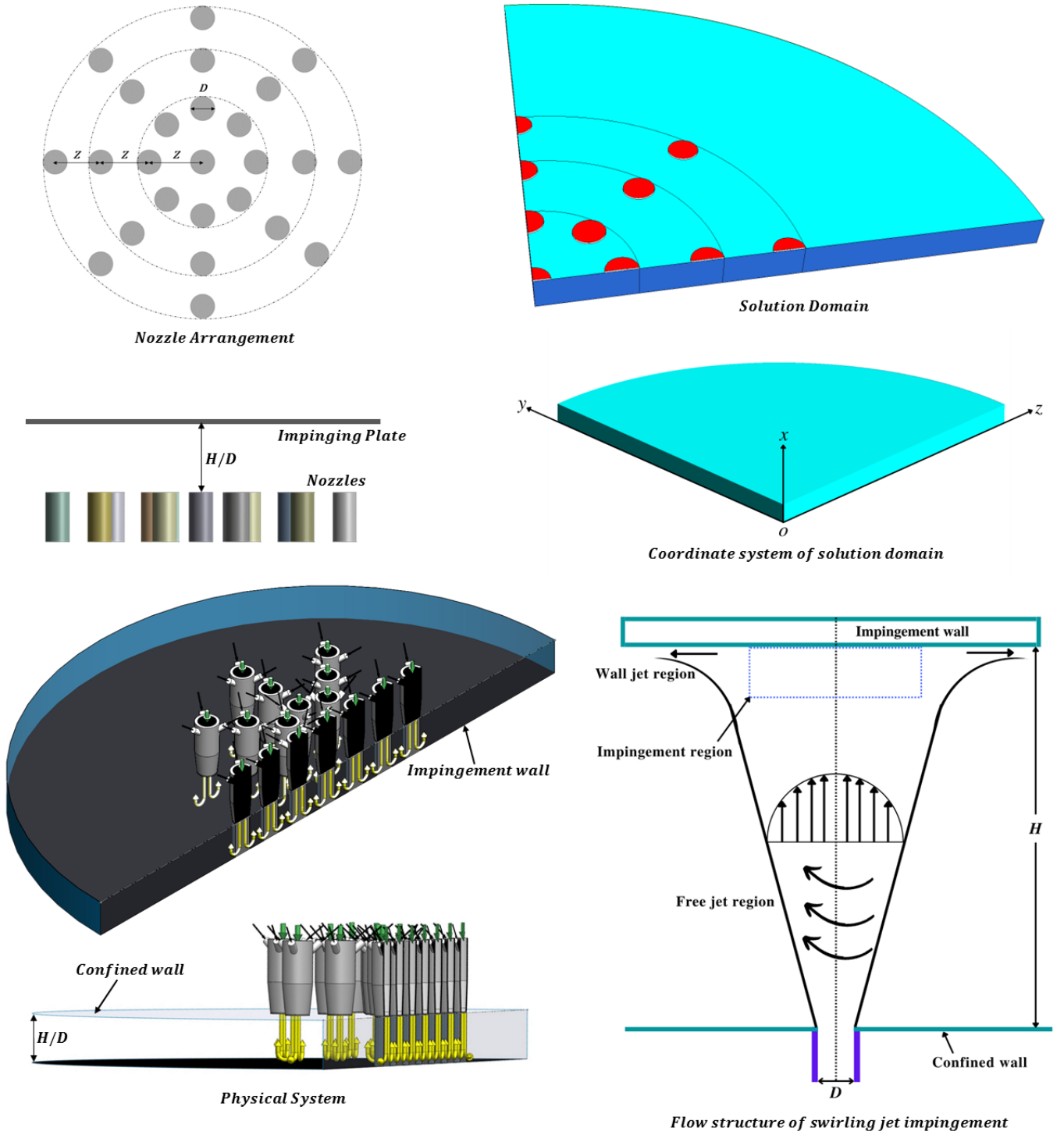

Fig. 1 A schematic view of the solution domain, the detailed of nozzles and coordinates, circular orientations of the inline nozzle arrangement, detailed illustrations of a physical system, and flow composition of the jet.

The governing equations to resolve the above 3*D* problem are the continuity equation, momentum equation, and energy equation. Turbulent flow is assumed to be resolved by the RANS approach. The governing equations in the compact form are:

$$\frac{\partial(\rho u\phi)}{\partial x}+\frac{\partial(\rho v\phi)}{\partial y}+\frac{\partial(\rho w\phi)}{\partial z}=\frac{\partial}{\partial x}\left(\Gamma_\phi\frac{\partial\phi}{\partial x}\right)+\frac{\partial}{\partial y}\left(\Gamma_\phi\frac{\partial\phi}{\partial y}\right)+\frac{\partial}{\partial z}\left(\Gamma_\phi\frac{\partial\phi}{\partial z}\right)+S_\phi \quad (1)$$

where ϕ, Γ_ϕ and S_ϕ represent the generalized variables, effective transport coefficients, and source terms, respectively. The detailed expressions for each of the governing equations are available in [20]. The turbulence closure terms $\overline{u'_i u'_j}$ and $u'_i T$ in Eq. (1) are expressed in indicial notations as:

$$\overline{u'_i u'_j}=2/3k\delta_{ij}-\mu_t\left(\frac{\partial u_i}{\partial x_j}+\frac{\partial u_j}{\partial x_i}\right) \quad (2)$$

$$\overline{u'_i T'}=-\Gamma_T\frac{\partial T}{\partial x_j} \quad (3)$$

where, μ_t is a function of k and ε or ω, which are determined via two other transport equations. The pressure velocity coupling was solved utilizing the coupled solver with Green-Gauss node-based gradient discretization. PRESTO is used for pressure discretization. Second-order upwind scheme for convective terms and second-order accurate (central difference) for diffusion terms of governing equations are applied. Residuals of each variable were set to 10^{-06}

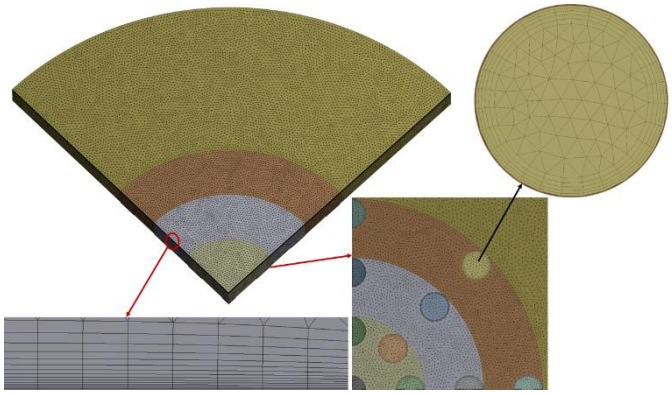

Fig. 2 Solution domain with detailed mesh in different sections.

A typical mesh for the current setup with an enlarged view of inflation layers, near the axis and inlet is shown in Fig. 2. Unstructured tetrahedral mesh with 15 prismatic layers near the surface and a growth rate of 1.2 is used to better resolve the wall characteristics. A relatively coarse mesh is created at the outer and upper boundaries of the area where variable flow is expected to be lower. A grid independence test was performed with five different numbers of nodes, namely 162k, 183k, 236k, 253k, and 293k. In this regard, the area-averaged Nusselt number is determined for circumferential area 6D of the plate for each mesh and the result of the grid independence study is presented in Table 1. It is observed that when the number of nodes is more than 236k, the variation of the area-averaged Nusselt number is less than 1%. To precisely acquire the numerical data as well as to minimize the computational cost, finally, 253k nodes were selected to execute the analysis. To accurately resolve the near-wall characteristics, the value of y+ is ensured less than unity for all cases almost in the whole simulation domain.

Table 1 Mesh independency test.

Mesh	Grid1	Grid2	Grid3	Grid4	Grid5
Elements	344805	461146	773292	842257	991763
Nodes	162830	183807	236374	253712	293480
$\overline{Nu}_{6D}$	120.38	120.71	121.38	122.14	122.16
y^+	1.29	1.22	1.06	0.98	0.88

Fig. 3 presents the applied boundary conditions on different locations of the solution domain. Boundary conditions in the simulation include the velocity of the inlet from each nozzle outlet, the non-slip and uniform state of the wall's heat flow, the atmospheric pressure on the inlet and outlet surfaces, and the adiabatic condition on the confined surface. Input conditions of different flow conditions (mean and turbulence) were obtained from the study by Ahmed [46]. Data profiles are set in all nozzles as input boundary conditions. The boundary symmetry state is applied to two side surfaces for non-swirling jets and periodic boundary conditions for swirling jets.

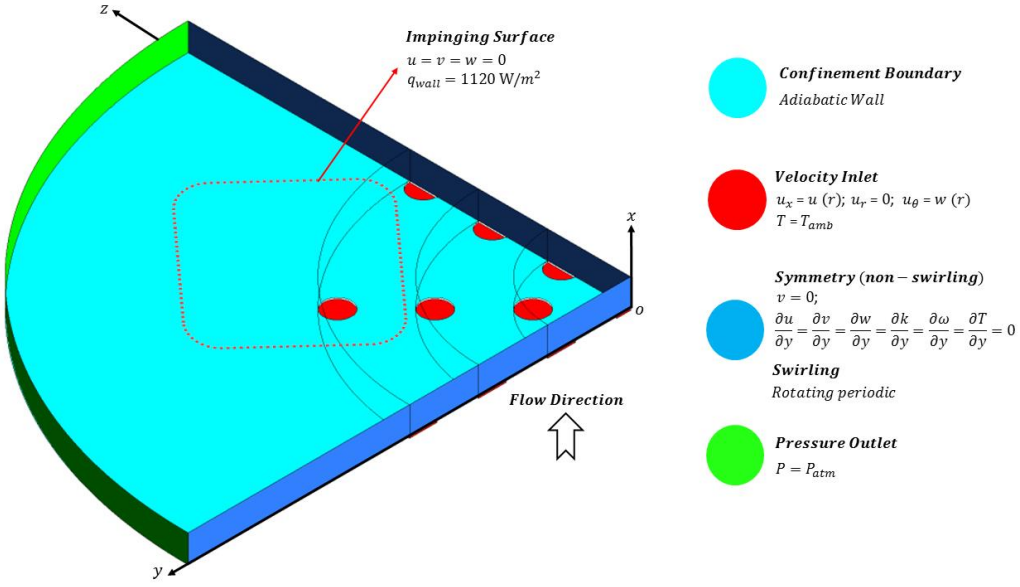

Fig. 3 Computational domain with detailed boundary conditions.

Lastly, Fig. 4 represents the numerical predictions of pressure coefficient (C_p) and surface heat transfer coefficient (h) at impinging plate along the radial line in the horizontal direction for single nozzle medium swirl (S = 0.3) flow at Re = 24600 and H = 1D using three different turbulence models (*SST k-ω*, Transition SST and Realizable *k-ε*) and they are compared with the experimental data [46]. In general, the numerical projections appropriately conform to the experimental data. However, in terms of surface heat transfer coefficient, slight variations among the numerical results and experimental data are visible which might be due to the differences in nozzle diameters, particular inlet conditions, and impinging distances. Furthermore, it is observed that *SST k-ω* is found to be in better agreement with the experimental data among all turbulence models. As such, the current research has considered the *SST k-ω* turbulence model for the computational analysis using a commercial software package ANSYS Fluent v17.

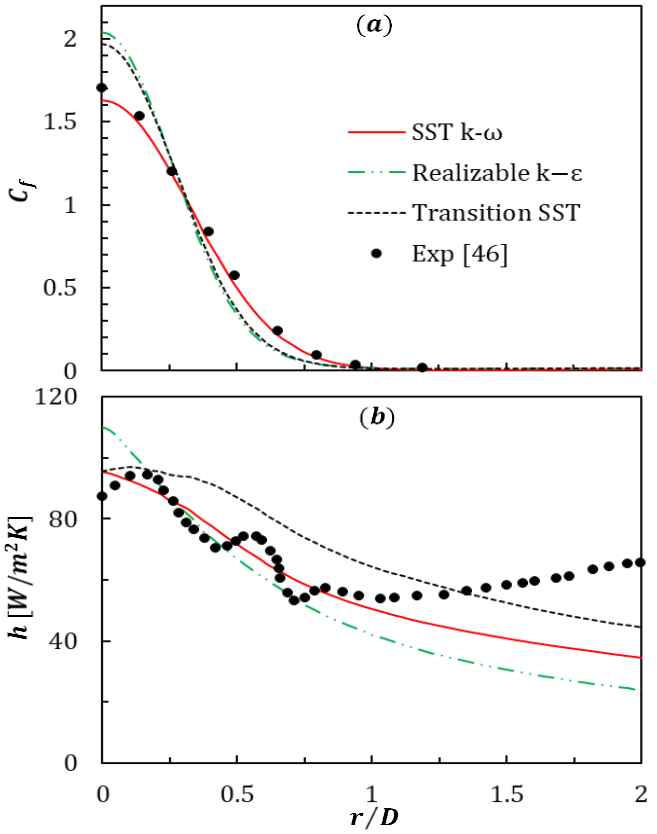

Fig. 4 Comparisons of (a) pressure coefficient (C_p) and (b) heat transfer coefficient (H) at impinging plate along the radial line in the horizontal direction for single nozzle medium swirl flow (S = 0.3) at Re = 24600 and H = 1D using different turbulence models.

3 Data Reduction

$$\overline{Nu} = \frac{1}{A}\int Nu dA \tag{4}$$

$$\eta = \frac{\overline{Nu}/\overline{Nu_o}}{f/f_o} \tag{5}$$

$$\overline{Nu} = 0.408 Re^{0.583}\left(\frac{H}{D}\right)^{-0.35} S^{0.18} \text{ [When } S = 0.3 \text{ \& } 0.75\text{]} \tag{6}$$

4 Results and Discussion

For the analysis of the coefficient of pressure C_p, data are taken at five planes (x/D = 0.2, 0.4, 0.6, 0.8, and 0.95) immediately after the nozzle exit close to the impingement surface. The results are shown in Fig. 5 for both medium and higher swirling flows when H = 1D and Re = 24600. The results for the medium-swirl flow show that the pressure adjacent to the nozzle exit is the lowest and gradually increases towards the impact plate. The results also show that the pressure is highest in areas of stagnation, where the flow impinges on the plate and then decreases radially and circumferentially. For S = 0.75, the static pressure in the nozzles gradually increases towards the impingement plate, similar to the medium-swirling jets. The pressure is comparatively more uniformly distributed across the impact plate in a higher swirling flow rather than a medium swirl.

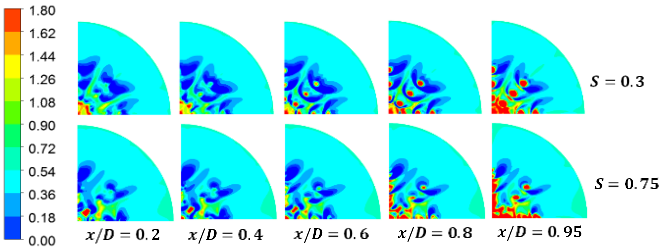

Fig. 5 Contours of pressure coefficient C_p at different axial distances of jets when S = 0.3 and 0.75 at H/D = 1 and Re = 24600.

Fig. 6 shows the velocity contours for S = 0.3 and 0.75 at different cross-sections in the axial direction for Re = 11600 and 35000. It can be seen from the figure that the jet velocity is maximum at the vicinity of the nozzle exit and it gradually decreases towards the impingement surface. The decreasing tendency for a higher swirling jet (S = 0.75) is stronger than for a medium-swirling jet (S = 0.3). The difference in velocity magnitude between Reynolds number 11600 and 35000 near the impingement surface is significant for higher-swirling jets, where Re = 35000 shows a larger magnitude.

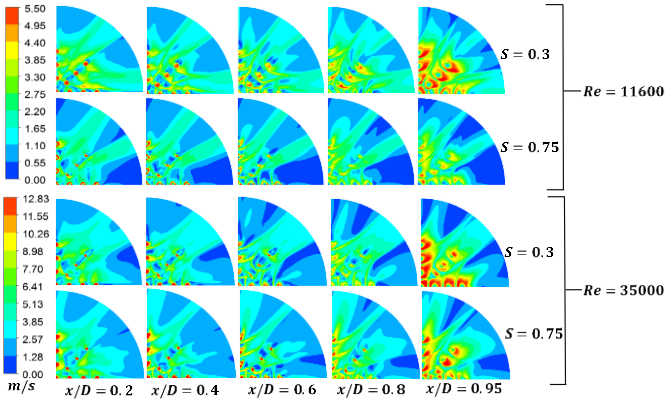

Fig. 6 Velocity contours at different axial distances of jets when S = 0.3 and 0.75 at H/D = 1 and Re = 11600 and 35000.

Fig. 7 shows the Nusselt number contours of adiabatic confined surface for both swirl flows at Reynolds number, Re = 11600, 24600, and 35000 when H/D = 0.25 and r/D = 5.5. Nusselt number is defined here as, $Nu = \frac{hD}{K}$, while h is the convective heat transfer coefficient, D is the diameter of the jet and K is the thermal conductivity of the fluid. Here, the same color scale is used for all contours. The result shows that changes

in local *Nu* distribution are evident only at *r/D* = 0 to 3 for all cases. Constant *Nu* is observed beyond that radial distance. However, these changes in heat transfer distribution due to confinement aren't evident for non-confined multiple impinging jets studies in the literature [23], [47], [48].

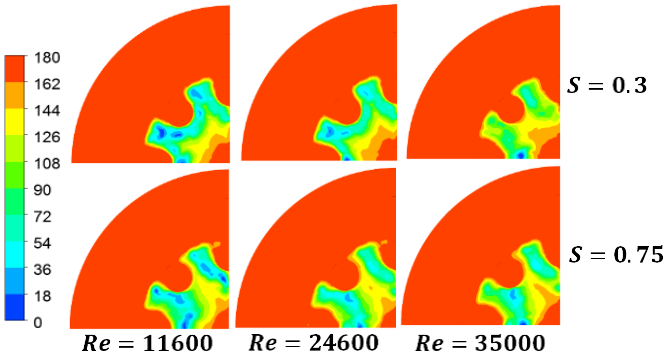

Fig. 7 Local Nusselt number recorded at confined surfaces when *S* = 0.3 and 0.75 at *H/D* = 0.25 and *Re* = 11600, 24600 and 35000.

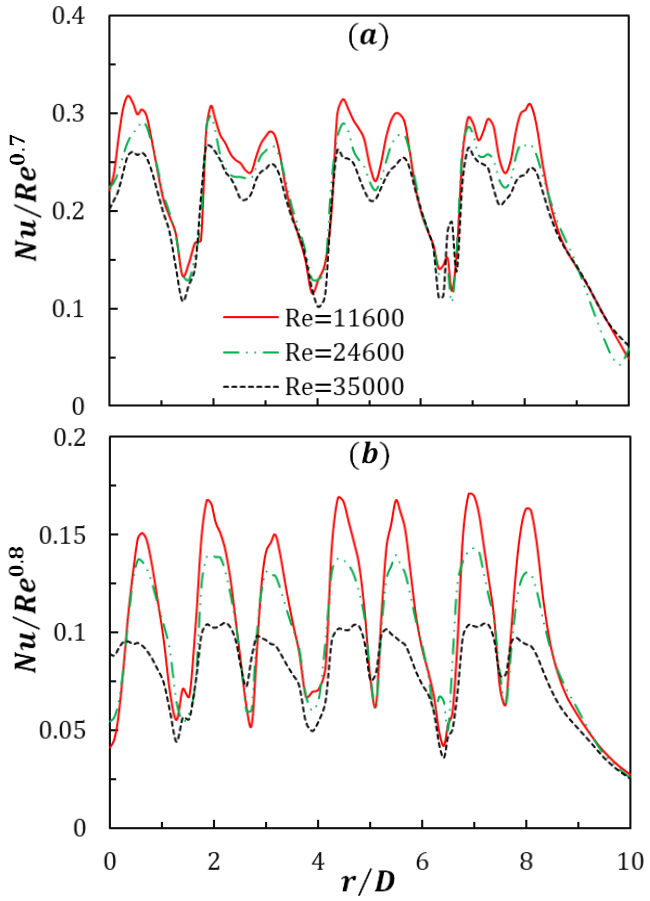

Fig. 8 The effect of Reynolds number and swirl number at *H* = 0.5*D* on heat transfer distribution: (a) *S* = 0.3 and (b) *S* = 0.75.

Circumferential area-averaged surface Nusselt number ($\overline{Nu}$) is determined for all cases using Eq. (4), where *A* is the circumferential area on the impingement surface. Three circumferential areas of radius 8*D*, 12*D*, and 16*D* are chosen for their relative comparison and the results are presented in Table 2. Here, $\overline{Nu}$ decreases with the increase of averaging area, since local *Nu* decrease monotonically after 8*D* according to Fig. 8. For both medium and higher swirling cases, better heat transfer performance is achieved for maximum Reynolds number and minimum impingement distance.

Table 2 Circumferential area-averaged Nusselt number $\overline{Nu}$ for both medium and higher swirling jets. Averaging is done for three different circumferential areas, namely 8*D*, 12*D* and 16*D*.

No.	*S*	*H/D*	***Re* = 11600** $\overline{Nu}$		
			8D	*12D*	*16D*
1	0.3	0.25	119.99	88.13	40.06
2		0.5	90.37	65.59	27.62
3		1	82.44	69.28	28.02
4	0.75	0.25	146.87	105.68	41.53
5		0.5	107.46	76.46	26.77
6		1	82.36	65.69	23.98
No.	*S*	*H/D*	***Re* = 24600** $\overline{Nu}$		
			8D	*12D*	*16D*
7	0.3	0.25	195.53	143.41	64.56
8		0.5	146.23	107.25	45.30
9		1	135.48	113.84	45.35
10	0.75	0.25	256.09	185.50	74.92
11		0.5	184.08	131.38	47.18
12		1	151.63	122.51	45.83
No.	*S*	*H/D*	***Re* = 35000** $\overline{Nu}$		
			8D	*12D*	*16D*
13	0.3	0.25	236.62	173.76	78.21
14		0.5	173.00	125.68	47.45
15		1	168.85	135.42	49.64
16	0.75	0.25	281.66	204.27	85.76
17		0.5	197.39	142.49	53.94
18		1	166.82	137.72	51.74

To analyze the effects of Reynolds number on the radial uniformity of Nusselt number distributions, Fig. 8 represents the data for swirl numbers *S* = 0.3 and 0.75 at *H* = 0.5*D* (*Re* = 11,600 – 35,000). To normalize the effect of various Reynolds numbers among the data sets, radial *Nu* values are scaled by Re^n along the radial profile. For both medium and higher swirl flows, the values of n are respectively, n = 0.7 and 0.8 which are also implemented and proposed by literature [6], [20], [49]. Here, a slight variation in the normalized *Nu* exists for *S* = 0.3 at multiple radial locations. This deviation may be attributed to differing characteristics of large-scale secondary vortex rings and their influences on surface heat transfer near the impingement wall. However, in the case of higher swirl flow, greater deviations are noticeable for *Re* = 35000 from the results of *Re* = 11600 and 24600. These may be because of the formation of severer recirculation zones and strong swirl intensities in case of maximum Reynolds number and swirl number near the impingement wall. Besides, a gradual decrease of *Nu* is observed for all cases after 8*D*.

Table 3 provides information regarding thermal performance factors for different Reynolds numbers and swirl numbers at multiple impinging distances. The thermal performance factor is derived by the ratio of the relative Nusselt number to the relative friction factor as visible in Eq. (5). It is observed that maximum η is achieved at the highest impinging distances for all Reynolds numbers and swirl cases. Besides, a higher Reynolds number ensured better thermal efficiency for both medium and higher swirling flows.

Table 3 Thermal performance factors (TPF) for different cases.

Re	S	H/D	TPF
11600	0.3	0.25	0.94252
		0.5	0.88956
		1	1.17701
	0.75	0.25	1.01197
		0.5	0.95872
		1	1.34364
24600	0.3	0.25	0.98754
		0.5	1.11463
		1	1.16170
	0.75	0.25	0.89286
		0.5	0.99308
		1	1.24030
35000	0.3	0.25	1.03308
		0.5	1.18371
		1	1.24031
	0.75	0.25	1.04963
		0.5	1.21446
		1	1.58675

To analyze the effects of Reynolds number on the radial uniformity of wall pressure distributions, Fig. 9 represents the data for swirl numbers S = 0.3 and 0.75 at H = 0.5D (Re = 11,600 – 35,000). As the coefficient of pressure can't be used as a dimensionless parameter to compare pressures on impingement wall surfaces at different Reynolds numbers due to the varying dynamic pressures in each case, the wall static pressure is normalized by the maximum pressure in the radial spread out for each given swirl number. The static pressure is found to be almost independent of Re for both medium and higher swirling cases when Re = 11600 and 24600. Here, a slight variation in the normalized P exists for S = 0.3 at r/D = 0.5 – 2; 4.5 – 5.5, and 7 – 8 when Re = 35000. For maximum (S = 0.75) swirl jet and Re = 35000, these variations are evident at r/D = 2.5 – 3.5; 4.5 – 5.5, and 7.5 – 8. These deviations may be allocated to differing properties of large-scale secondary vortex rings and their contributions to the downstream flow organization at the impingement region. No significant change in static pressure distribution is evident after r/D = 8.5.

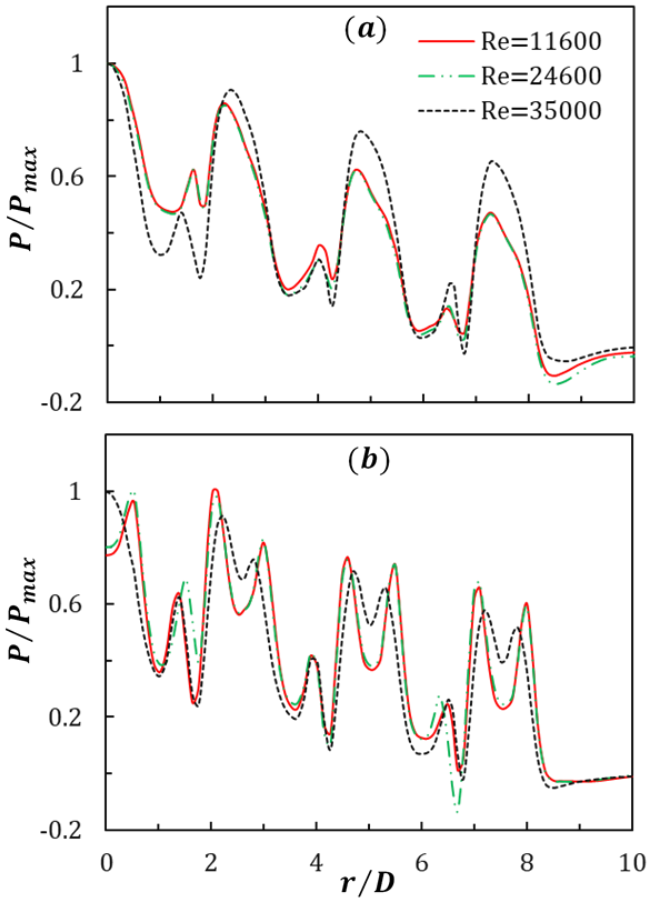

Fig. 9 The effect of Reynolds number and swirl number at H = 0.5D on impingement pressure distribution: (a) S = 0.3 and (b) S = 0.75.

Fig. 10 represents the radial distribution of Reynolds normal stress along the axial direction for the inline arrangement of nozzles at Re = 35000 for medium (S = 0.3) and high swirl (S = 0.75) flow. It is observed that for medium swirl flow all the normal stress components $\overline{u'u'}$, $\overline{v'v'}$, $\overline{w'w'}$ at each axial plane are maximum at the location of the nozzles and where the nozzle is not located the stress is low. Moreover, the intensity of the stress is proportional to the axial location i.e. normal stress adjacent to the plane of nozzle exit is more intense relative to the outlying planes. Due to the high flow pressure of the jet, the normal stress at the nozzle vicinity is intense. For high swirl flow, the normal shear stress shows an unpredictable nature due to the high swirl intensity. The $\overline{v'v'}$, and $\overline{w'w'}$ component of the normal stress are intense at the furthest position from the nozzle exit where the $\overline{u'u'}$ component is intense at the x/D = 0.5. The magnitude of normal shear stress is found maximum adjacent to the 3rd and 4th series of nozzles, where at the first and second nozzle the stress is not intense. This can be attributed to the strong recirculation vortex due to the high swirl flow which occurs at r/D = 4-5 and 6.5-7.5.

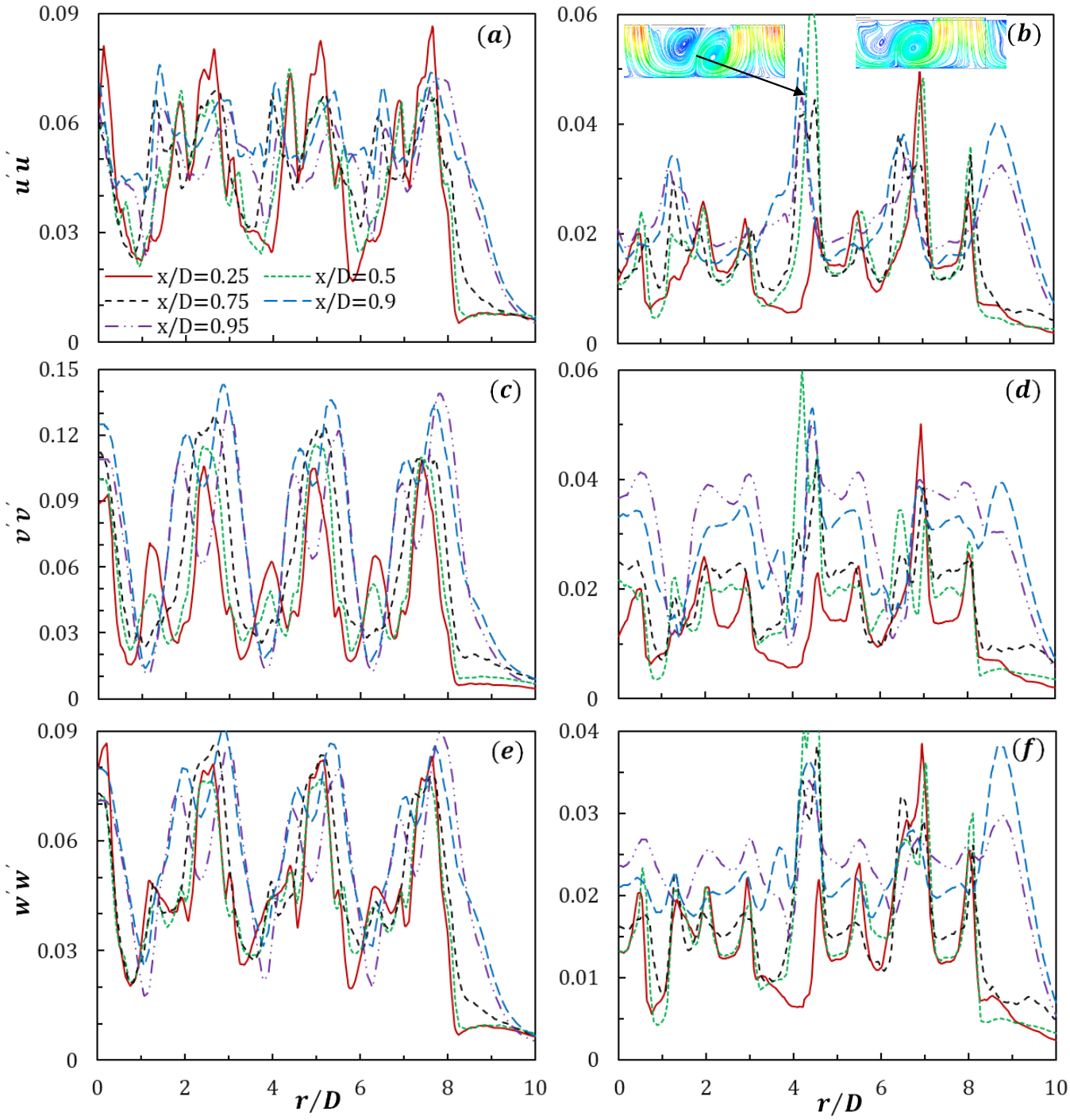

Fig. 10 Radial distribution of Reynolds normal stress along different axial planes at *Re* = 35000 and *H/D* = 1 for (a, c, e) *S* = 0.3 and (b, d, f) *S* = 0.75.

Fig. 11 represents the radial distribution of Reynolds shear stress along the axial direction for the inline arrangement of nozzles at *Re* = 35000 at *H/D* = 1 for medium (*S* = 0.3) and high swirl (*S* = 0.75) flow. It is observed that the Reynolds shear stress shows a very unpredictable nature due to the effect of the swirl. The $u'v'$ component of shear stress at *x/D* = 0.5 is comparatively more intensive than other locations for medium swirl flow. The magnitude of shear stress $u'v'$ component at the nozzle location is low. On the contrary, in the case of high swirl flow the $u'v'$ component of shear stress at *x/D* = 0.9 is more intensive. However, near the 3rd series of the nozzle the $u'v'$ component of shear stress at *x/D* = 0.25 and *x/D* = 0.5 suddenly become high. The $u'w'$ component of shear stress at the nozzle location is high for both medium and high swirl flow conditions. Moreover, the magnitude of the stress at the vicinity of the nozzle exit is more intense compared to the outlying planes. The $v'w'$ component of shear stress is minimum at the nozzle location for medium swirl flow and the intensity of the stress near the nozzle exit plane is high. For high swirl flow, the stress at *r/D* = 5-7 suddenly becomes very high.

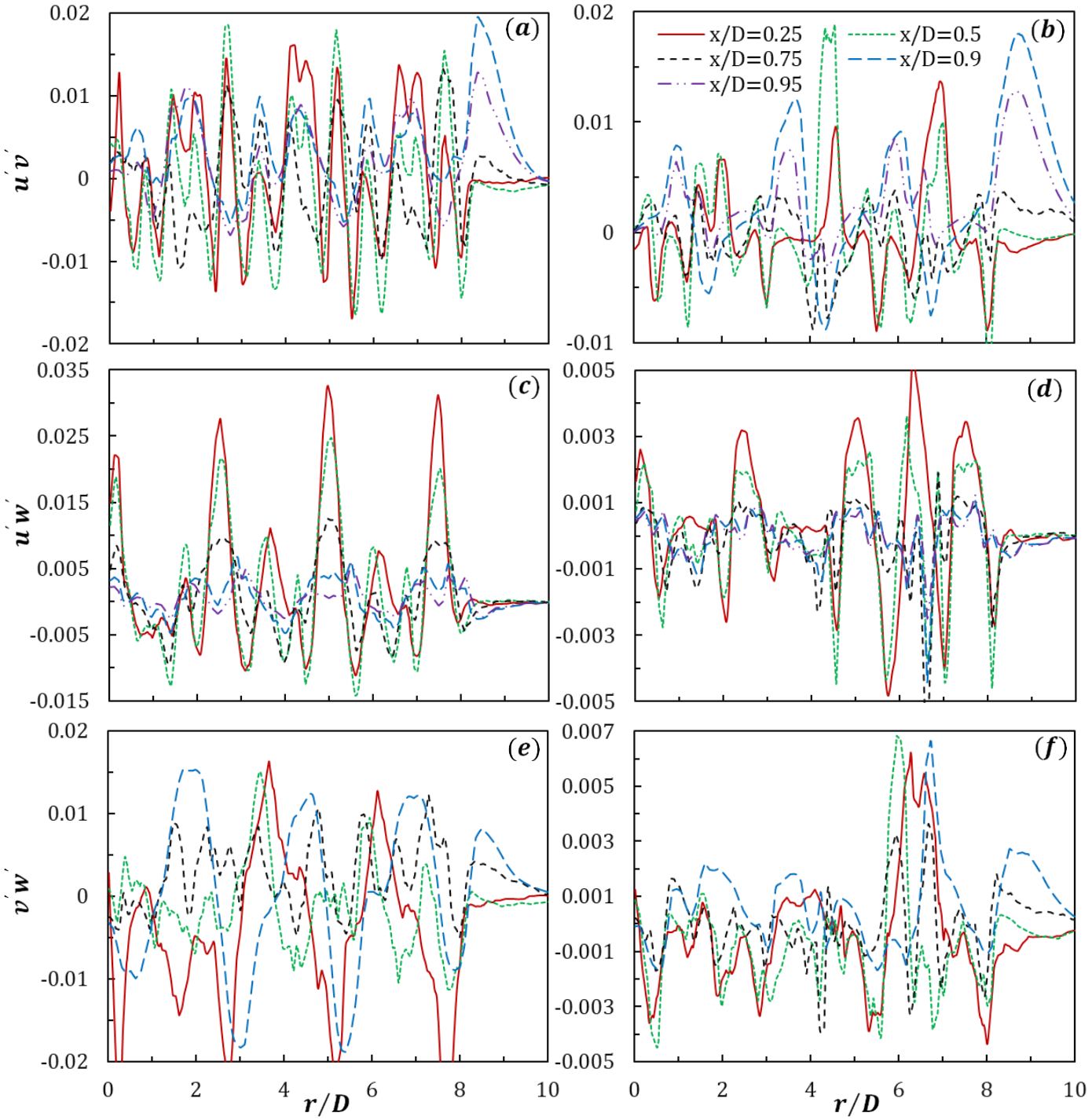

Fig. 11 Radial distribution of Reynolds shear stress along the axial direction of the impinging plate at *Re*= 35000 at *H/D* = 1 for (a, c, e) *S* = 0.3 and (b, d, f) *S* = 0.75.

Heat transfer for all cases is predicted by using multivariate regression analysis on the commercial software package IBM SPSS. The proposed correlation relates to all Reynolds numbers, impinging distances, and swirl numbers. The founded correlation equation for area average $\overline{Nu}$ is given as Eq. (6). Fig. 12 portrayed the virtue of every fit by plotting ±10% error bands with comparisons between the numerical values and predicted ones by Eq. (6). The obtained R^2 value for the correlation is 0.952 and it is visible that, most predictions stay within both error bands. This shows that the proposed correlation is acceptable for the considered cases in the current study. Numerous cases are considered in the current study along with the different flow and geomatics parameters. Consequently, it's necessary to investigate the outcomes in terms of possible enhancement factors. As such, the Circumferential area-averaged surface Nusselt number ($\overline{Nu}$) and thermal performance factor (TPF) are tested for an increase of swirl intensity from medium (*S* = 0.3) to high (*S* = 0.75), while *Re* = 11600 and *H/D* = 0.5. 19% and 8% raises are predicted in terms of $\overline{Nu}$ and TPF respectively. Furthermore, both parameters are tested with the change of Reynolds number from 11600 to 35000 while *S* = 0.75 and *H/D* = 1. Around 102% and 23% increments are found in terms of $\overline{Nu}$ and TPF respectively.

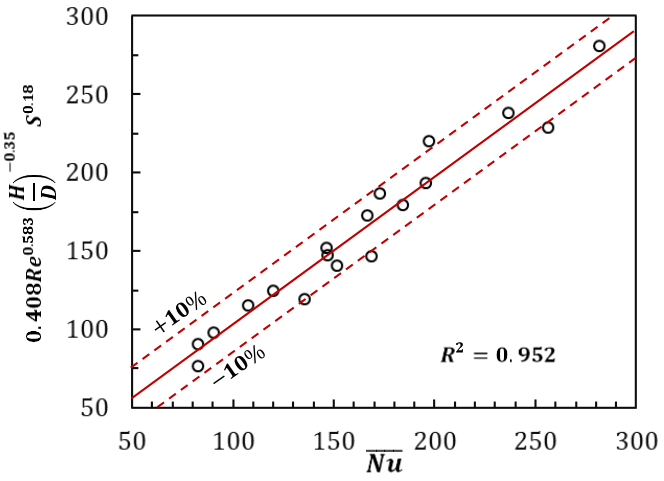

Fig. 12 Contrast among the simulation data and the correlated results for area average Nusselt number (*Nu*) with error bands.

5 Conclusion

A numerical study has been conducted to investigate the thermo-fluidic characteristics of a swirl-impinging jet emanating from an aerodynamic swirl nozzle for various flow and geometric conditions. The flow parameters are selected based on Reynolds numbers, impinging distance, swirl number, and jet-to-jet separation distances. The analysis is conducted using the SST k-ω turbulence model, and various flow and thermal behaviors are observed. The results of this analysis are summarized below:

- The static pressure at the stagnation region is very high for both the low and high swirl flows and gradually decreases with the radial and circumferential distance. Moreover, static pressure adjacent to the nozzle exit is low and increases gradually with the impinging distance. Pressure distribution along the impingement surface is more uniform in case of high swirl flow. Besides, the static pressure is found independent of the Reynolds number for both the low and high swirl flow at a low Reynolds number. However, for a high Reynolds number, significant variation of static pressure is observed due to the influence of the large-scale secondary vortex downstream to the impingement region.
- The jet velocity is maximum at the vicinity of the nozzle exit and decelerates gradually towards the impingement surface. This receding tendency is relatively stronger for high swirl flow than the low swirl conditions.
- Local Nusselt number at the confinement surface is varying at a radial distance of 0 to 3 for all the flow conditions and beyond that distance, the Nusselt number is found constant. Moreover, the heat transfer characteristic at the confined surface is different from the non-confined ones. Nusselt number at the stagnation region is very high which accelerates with the Reynolds number and swirl number due to the increased flow velocity and turbulence, respectively. The average Nusselt number decreases with the increment of the circumferential area on the impinging surface and maximum heat transfer performance is evident at the minimum impinging distance. Moreover, a correlation is established for the area average Nusselt numbers for all the considered cases in the current study.
- Reynolds normal stress adjacent to the nozzle exit is more intensive compared to the outlying planes due to the high flow pressure of the jet while the Reynolds shear stress along the radial direction is changing unpredictably due to the influence of the recirculating vortex.
- An estimated 102% enhancement in average Nusselt number is observed for high swirl flow, at a Reynolds number increment from 11600 to 35000. This enhancement is evident by 23% in terms of thermal performance factor. Besides, the average Nusselt number and thermal performance factor augmented by 19% and 8%, respectively, for an increased swirl intensity at low a Reynolds number (*Re* =11600).

References

[1] Röger, M., Buck, R. and Müller-Steinhagen, H., 2005. Numerical and experimental investigation of a multiple air jet cooling system for application in a solar thermal receiver.

[2] Han, J.C., 2004. Recent studies in turbine blade cooling. *International journal of rotating machinery*, *10*(6), pp.443-457.

[3] Becko, Y., 1976. Impingement Cooling—A Review, *Von Karman Institute for Fluid Dynamic*, Lecture Series 83, Turbine Blade Cooling.

[4] Hall, C.W., 1988. Handbook of industrial drying, *Dry. Technol.* *6*(3), pp. 571–573.

[5] Yang, L., Ren, J., Jiang, H. and Ligrani, P., 2014. Experimental and numerical investigation of unsteady impingement cooling within a blade leading edge passage. *International Journal of Heat and Mass Transfer*, *71*, pp.57-68.

[6] Martin, H., 1977. Heat and mass transfer between impinging gas jets and solid surfaces. In *Advances in Heat Transfer*, 13, pp. 1-60, Elsevier.

[7] Colucci, D.W. and Viskanta, R., 1996. Effect of nozzle geometry on local convective heat transfer to a confined impinging air jet. *Experimental Thermal and Fluid Science*, *13*(1), pp.71-80.

[8] Saad, N.R., Polat, S. and Douglas, W.J.M., 1992. Confined multiple impinging slot jets without crossflow effects. *International Journal of Heat and Fuid Flow*, *13*(1), pp.2-14.

[9] Huber, A.M. and Viskanta, R., 1994. Convective heat transfer to a confined impinging array of air jets with spent air exits. *J. Heat Transfer*, *116*(3), pp. 570-576.

[10] Markal, B., 2018. Experimental investigation of heat transfer characteristics and wall pressure distribution of swirling coaxial confined impinging air jets. *International Journal of Heat and Mass Transfer*, *124*, pp.517-532.

[11] Markal, B., 2019. The effect of total flowrate on the cooling performance of swirling coaxial impinging jets. *Heat and Mass Transfer*, *55*(11), pp.3275-3288.

[12] Habib, M.A. and Whitelaw, J.H., 1980. Velocity characteristics of confined coaxial jets with and without swirl. *J. Fluids Eng.* *102*(1), pp. 47-53.

[13] Memar, H., Holman, J.P. and Dellenback, P.A., 1993. The effect of a swirled annular jet on convective heat transfer in confined coaxial jet mixing. *International Journal of Heat and Mass Transfer*, *36*(16), pp.3921-3930.

[14] Petera, K. and Dostál, M., 2017. Heat transfer in a confined impinging jet with swirling velocity component. In *EPJ Web of Conferences*, 143, p. 02091. EDP Sciences.

[15] Shuja, S.Z., Yilbas, B.S. and Rashid, M., 2003. Confined swirling jet impingement onto an adiabatic wall. *International Journal of Heat and Mass Transfer*, *46*(16), pp.2947-2955.

[16] Chouaieb, S., Kriaa, W., Mhiri, H. and Bournot, P., 2017. Swirl generator effect on a confined coaxial jet characteristics. *International Journal of Hydrogen Energy*, *42*(48), pp. 29014-29025.

[17] Liu, L., Zhang, J., Liu, S., Wang, K. and Gu, H., 2021. Decay law and swirl length of swirling gas-liquid flow in a vertical pipe. *International Journal of Multiphase Flow*, *137*, p.103570.

[18] Yan, J., Gui, N., Xie, G. and Gao, J., 2014. Direct numerical simulation and visualization of biswirling jets. *Advances in Mechanical Engineering*, *6*, p.193731.

[19] Fénot, M., Dorignac, E. and Lalizel, G., 2015. Heat transfer and flow structure of a multichannel impinging jet. *International Journal of Thermal Sciences*, *90*, pp.323-338.

[20] Ahmed, Z.U., Al-Abdeli, Y.M. and Guzzomi, F.G., 2017. Flow field and thermal behaviour in swirling and non-swirling turbulent impinging jets. *International Journal of Thermal Sciences*, *114*, pp.241-256.

[21] Ahmed, Z.U., Al-Abdeli, Y.M. and Matthews, M.T., 2015. The effect of inflow conditions on the development of non-swirling versus swirling impinging turbulent jets. *Computers & Fluids*, *118*, pp.255-273.

[22] Wu, F., Li, L., Wang, J., Fan, X. and Du, C., 2019. Numerical investigations on flow and heat transfer of swirl and impingement composite cooling structures of turbine blade leading edge. *International Journal of Heat and Mass Transfer*, *144*, p. 118625.

[23] Debnath, S., Khan, M.H.U. and Ahmed, Z.U., 2020. Turbulent swirling impinging jet arrays: A numerical study on fluid flow and heat transfer. *Thermal Science and Engineering Progress*, *19*, p. 100580.

[24] Debnath, S., Khan, M.H.U., Ahmed, Z.U. and Alam, M.M., 2018. The effect of swirl on array of turbulent impinging jets. In *International Conference on Mechanical, Industrial and Energy Engineering*, December, 2018, Khulna, Bangladesh.

[25] Debnath, S. and Ahmed, Z.U., 2020. Computational analysis of multiple non-swirling & swirling impinging air jets. In *International Conference on Mechanical, Industrial and Energy Engineering*, December, Khulna, Bangladesh.

[26] Wannassi, M. and Monnoyer, F., 2015. Fluid flow and convective heat transfer of combined swirling and straight impinging jet arrays. *Applied Thermal Engineering*, *78*, pp.62-73.

[27] Hollworth, B.R., Lehmann, G. and Rosiczkowski, J., 1983. Arrays of impinging jets with spent fluid removal through vent holes on the target surface, part 2: local heat transfer.

[28] Zhang, J., Sun, Y., Li, J. and He, X., 2020. Study on the hybrid cooling of the flame tube in a small triple-swirler combustor. *Energies*, *13*(21), p. 5554.

[29] Wu, F., Li, L., Wang, J., Fan, X. and Du, C., 2019. Numerical investigations on flow and heat transfer of swirl and impingement composite cooling structures of turbine blade leading edge. *International Journal of Heat and Mass Transfer*, *144*, p. 118625.

[30] Caliskan, S. and Baskaya, S., 2012. Experimental investigation of impinging jet array heat transfer from a surface with V-shaped and convergent-divergent ribs. *International Journal of Thermal Sciences*, *59*, pp. 234-246.

[31] Chauhan, R. and Thakur, N.S., 2013. Heat transfer and friction factor correlations for impinging jet solar air heater. *Experimental Thermal and Fluid Science*, *44*, pp.760-767.

[32] Hatami, M., Bazdidi-Tehrani, F., Abouata, A. and Mohammadi-Ahmar, A., 2018. Investigation of geometry and dimensionless parameters effects on the flow field and heat transfer of impingement synthetic jets. *International Journal of Thermal Sciences*, *127*, pp.41-52.

[33] Wang, C., Wang, Z., Wang, L., Luo, L. and Sundén, B., 2019. Experimental study of fluid flow and heat transfer of jet impingement in cross-flow with a vortex generator pair. *International Journal of Heat and Mass Transfer*, *135*, pp. 935-949.

[34] Katti, V.V., Yasaswy, S.N. and Prabhu, S.V., 2011. Local heat transfer distribution between smooth flat surface and impinging air jet from a circular nozzle at low Reynolds numbers. *Heat and Mass Transfer*, *47*(3), pp. 237-244.

[35] Jeffers, N., Stafford, J., Conway, C., Punch, J. and Walsh, E., 2016. The influence of the stagnation zone on the fluid dynamics at the nozzle exit of a confined and submerged impinging jet. *Experiments in Fluids*, *57*(2), pp. 1-15.

[36] Ekkad, S.V. and Han, J.C., 2000. A transient liquid crystal thermography technique for gas turbine heat transfer measurements. *Measurement Science and Technology*, *11*(7), p. 957.

[37] Ichikawa, Y., Motosuke, M., Kameya, Y., Yamamoto, M. and Honami, S., 2016. Three-dimensional flow characterization of a square array of multiple circular impinging jets using stereoscopic PIV and heat transfer relation. *Journal of Visualization*, *19*(1), pp. 89-101.

[38] Buzzard, W.C., Ren, Z., Ligrani, P.M., Nakamata, C. and Ueguchi, S., 2017. Influences of target surface small-scale rectangle roughness on impingement jet array heat transfer. *International Journal of Heat and Mass Transfer*, *110*, pp. 805-816.

[39] Ligrani, P.M., Ren, Z. and Buzzard, W.C., 2017. Impingement jet array heat transfer with small-scale cylinder target surface roughness arrays. *International Journal of Heat and Mass Transfer*, *107*, pp. 895-905.

[40] Singh, D., Premachandran, B. and Kohli, S., 2015. Circular air jet impingement cooling of a circular cylinder with flow confinement. *International Journal of Heat and Mass Transfer*, *91*, pp. 969-989.

[41] Caggese, O., Gnaegi, G., Hannema, G., Terzis, A. and Ott, P., 2013. Experimental and numerical investigation of a fully confined impingement round jet. *International Journal of Heat and Mass Transfer*, *65*, pp. 873-882.

[42] Manca, O., Cirillo, L., Nardini, S., Buonomo, B. and Ercole, D., 2016. Experimental investigation on fluid dynamic and thermal behavior in confined impinging round jets in aluminum foam. *Energy Procedia*, *101*, pp. 1095-1102.

[43] Islam, S.M., Khan, M.T. and Ahmed, Z.U., 2020. Effect of design parameters on flow characteristics of an aerodynamic swirl nozzle. *Progress in Computational Fluid Dynamics, an International Journal*, *20*(5), pp. 249-262..

[44] Khan, M.T., Islam, S.M. and Ahmed, Z.U., 2020. Near-wall and turbulence behavior of swirl flows through an aerodynamic nozzle. *Journal of Engineering Advancements*, *1*(2), pp. 43-52.

[45] Khan, T. and Ahmed, Z.U., 2022. Effect of nanofluids on heat transfer characteristics of an aerodynamic swirl nozzle for isothermal and isoflux conditions. *Australian Journal of Mechanical Engineering*, pp. 1-19.

[46] Ahmed, Z.U., 2016. An experimental and numerical study of surface interactions in turbulent swirling jets. *Dissertation submitted for the degree of Doctor of Philosophy, School of Engineering*, Edith Cowan University, Australia.

[47] Debnath, S., Ahmed, Z.U., Ikhlaq, M. and Khan, T., Thermal characteristics of arrays of swirling impinging jets: Effect of Reynolds number, impingement distance, and jet-to-jet separation. *Heat Transfer*, *51*(1), pp. 585-608.

[48] Khan, T., Debnath, S., Ahmed, Z. U., & Islam, S.M., 2022. Effects of impinging distance, reynolds number, and swirl on the flow and heat transfer behaviors of arrays of circular impinging jets: A numerical approach. In *International Conference on Mechanical, Industrial and Energy Engineering* December, Khulna, Bangladesh.

[49] Ahmed, Z.U., Al-Abdeli, Y.M. and Guzzomi, F.G., 2016. Heat transfer characteristics of swirling and non-swirling impinging turbulent jets. *International Journal of Heat and Mass Transfer*, *102*, pp. 991-1003.